Supplementary Methods and Notes

Beyond Six Feet: A Guideline to Limit Indoor Airborne Transmission of COVID-19

Martin Z. Bazant,[1,2*] and John W. M. Bush[2]

[1]Department of Chemical Engineering [2]Department of Mathematics

Massachusetts Institute of Technology, Cambridge, MA 02139, USA

[*]To whom correspondence should be addressed; E-mail: bazant@mit.edu.

S1 Deduction of the indoor safety guideline from epidemiological models

In this section, we demonstrate that our indoor safety guideline (Eq. 3) may be deduced from standard epidemiological models.

While our theoretical model of the well-mixed room was developed to describe airborne transmission from a single individual to a fixed number of others in a well-mixed room, it bears noting that this scenario is but one of a broader class of transmission events. First, there are many situations where air conditioning or forced ventilation mixes air between rooms, in which case the compound room is effectively a well-mixed space. Second, there are incidents when several individuals are initially infected. Third, the population may be together for a period long with respect to the incubation time (approximately 5.5 days [1]), in which case the number of infectious

individuals necessarily increases with time. Examples of this broader class of transmission events might include cruise ships [2–6], meat and poultry processing facilities [7,8] and prisons [9,10]. We proceed by detailing the epidemiological models describing this more general class of events.

Following Noakes et al.[11], we adopt the standard SEIR model from epidemiology [12,13], an extension of the original SIR model of Kermack and McKendrick[14] of susceptible (S), infected (I) and recovered (R) populations to include an exposed population (E) that has acquired the pathogen and so become infected but not yet infectious:

$$\frac{dS}{dt} = -\beta SI,\ \frac{dE}{dt} = \beta SI - \alpha E,\ \frac{dI}{dt} = \alpha E - \gamma I,\ \frac{dR}{dt} = \gamma I \tag{S1}$$

where α is the incubation rate, $\beta(t)$ is the transmission rate, and γ is the recovery rate of the infected. To describe a spreading event in a closed environment, we consider I_0 infected people entering, at time $t = 0$, a room full of $S_0 = N - I_0$ susceptible individuals, none of which were previously exposed, $E_0 = 0$. In the case where the population is being tested and infected individuals removed from the population via isolation, γ may alternatively be considered as a proxy for testing frequency. Noting that the combined incubation time and time to recovery for COVID-19 is thought to exceed 2 weeks [15], we here consider spreading events of duration τ that are short relative to the recovery time, $\tau \ll \gamma^{-1}$, and so eliminate R from consideration.

The Wells-Riley model is effectively a reduction of the SIR model based on the assumption of slow incubation over the timescale of the event, $\tau \ll \alpha^{-1}$, in which case the number of infected persons in the room remains fixed, $I(t) = I_0$. One expects such to be the case for events of relatively short duration, such as the Skagit Choir incident. However, such an approximation is

not likely to be valid in the case of indoor super-spreading events of longer duration, $\tau > \alpha^{-1}$. To adequately model such events, we consider the possibility that the number of infectors increases with time, which requires a description of the nonlinear dynamics of disease transmission.

The resulting SEI model to be considered here is a system of three nonlinear ordinary differential equations. While the system may be solved numerically, deduction of a safety guideline requires analytical results. Our goal is thus to solve this SEI model for the infection (or "secondary attack") rate, $i_S(\tau) = (E(\tau)+I(\tau)-I_0)/S_0$. Since exact solutions may be cumbersome (as for the SIR model [16]), we simplify the analysis by considering two limits, where the incubation time α^{-1} is short or long relative to the event timescale, τ, and the transmission timescale β^{-1}. While the incubation time of COVID-19 is not precisely known, it is bounded above by the time to develop symptoms, which spans 2-14 days with an average 5.5 days [1].

For slow incubation ($\alpha \ll \beta, \tau^{-1}$) [11], the number of infected persons remains nearly constant, $I(t) \approx I_0$, and the resulting SE model is easily solved to derive the secondary attack rate [17],

$$i_S(\tau) = 1 - e^{-I_0 \int_0^\tau \beta(t)dt}, \tag{S2}$$

In the opposite limit of fast incubation ($\alpha \gg \beta, \tau^{-1}$), exposed individuals are rapidly infected, so the exposed, non-infected population need not be considered, $E(t) = 0$. Solving the resulting SI model yields

$$i_S(\tau) = \left[1 - i_0^{-1}\left(e^{N\int_0^\tau \beta(t)dt} - 1\right)^{-1}\right]^{-1}, \tag{S3}$$

where $i_0 = I_0/N$ is the initial percentage of infected individuals. These simple solutions, (S2) and (S3), cover the two limiting cases of fast and slow incubation relative to transmission.

The safety criterion $\mathcal{R}_{in} < \epsilon$, which limits the probability of the first transmission to lie below a small tolerance, is universal, in that it does not depend on the choice of model to describe the subsequent spreading dynamics. In particular, the safety criterion, $I(\tau) < 1 + \epsilon$, with $I_0 = 1$ corresponds to

$$\frac{\mathcal{R}_{in}}{N-1} = \int_0^\tau \beta(t)dt < \begin{cases} -\ln\left(1 - \frac{\epsilon}{N-1}\right) & \text{(slow)} \\ \frac{1}{N}\ln\left[\frac{(N-1)(1+\epsilon)}{N-1-\epsilon}\right] & \text{(fast)} \end{cases} \tag{S4}$$

according to Eqs. (S2) and (S3) for slow and fast incubation, respectively. In the small-tolerance limit, $\epsilon \ll 1$, these bounds both reduce to, $\mathcal{R}_{in} < \epsilon$, and are thus independent of the incubation rate. More generally, the linear response of any Markovian, mean-field theory (with neither memory nor many-body correlations) to any perturbation, such as the arrival of a new infector, must begin at the mean transmission rate. Indeed, the same universal bound may be simply derived from the infinitesimal cumulative probability of transmission $\int_0^\tau \beta(t)$ from one infector to a set of $N-1$ independent susceptibles.

S2 Inference of infection quanta from disease spreading data

It is an important point that the concentration of "infection quanta" per exhaled air volume, C_q, as may be inferred from spreading data, is necessarily *model dependent*. By definition, the time integral of the transmission rate, $q(t) = \int_0^\tau \beta(t)dt$, is equal to the expected number of quanta transferred from one infector to one susceptible. In models of indoor airborne transmission [11,17,18], infection quanta are further related to the evolving pathogen-laden droplet concentration by Eq. (4). While the mathematical definition of infection quantum is unambiguous in terms of the in-

stantaneous transmission rate, $\beta(t)$, between two isolated individuals, the inference of quanta concentrations from field data for the spreading rate is inevitably model-dependent because it involves interactions among an evolving population. Specifically, the long-time growth in the number of infections is influenced by nonlinearities in the transmission dynamics, as governed by the chosen epidemiological model, for example, the SEIR model, Eq. (S1).

In the original Wells-Riley model [11,17,19–21], one infection quantum is defined as the amount of pathogen required to infect an average of $1 - 1/e \approx 63.2\%$ of susceptible people in an enclosed space. This inference is based on fitting field data to Eq. (S2), which relates one net quantum transferred, $I_0 q(t) = 1$, to the secondary infection rate, $i_S(t) = 1 - (1/e)$. This approach is valid for times short relative to the incubation time and has been successfully applied to extract quanta emission rates for various viral diseases [22–25], including SARS-CoV-2 [18,26]. However, the Wells-Riley model cannot be reliably used to infer infection quanta from super-spreading events evolving over time scales that exceed the incubation time.

Here, we take an approach appropriate for the case of fast incubation that necessarily implies a different relation between released infection quanta and the observed secondary infection rate. If we adopt the SI model with fast incubation, then the long-term behavior of Eq. (S3) indicates that one quantum ($I_0 q(t) = 1$) will infect a fraction $i_S = [1 + (N/I_0)/(e^{N/I_0} - 1)]^{-1}$ of N people in an enclosed space, I_0 of which were initially infected, as a result of transmission amplification by the growing number of infectors. In this model, a single quantum from one person infects another with probability $i_S = [1 + 2/(e^2 - 1)]^{-1} \approx 76.2\%$ for $N = 2$, but manages to infect everyone in a large

group, $i_S \to 1$ as $N \to \infty$. This dependence of infection quanta on epidemiological model parameters, such as the incubation rate, reflects the fact that the fitted "infection quantum" is a measure of *contagiousness* at the scale of a group that is not necessarily proportional to the microscopic pathogen concentration. Notably, infection quanta are well defined in the limit of short times and slow transmission, where all models reduce to the Wells-Riley model with a constant number of infectors. From the modeling perspective, the notion of infection quanta is thus unambiguous only in this limit. Finally, we recall that, regardless of the model used to infer it, the actual value of infection quanta may still vary considerably between spreading events, owing to its dependence on activity level of the population and other physiological factors [18,27].

The Diamond Princess. The data reported for the Diamond Princess is particularly useful in that it captures the time evolution of the infected persons among a fixed population over an extended period, corresponding to the 12-day quarantine [3,4], after which passengers and crew began to disembark. The resulting data reported for $I(t)$ is best described in terms of the fast-incubation limit (Figure S1). Fitting to the available data allows us to infer that the initial number of passengers infected on February 3, 2020 was approximately $I_0 = 20$, and that the concentration of infection quanta characterizing this particular spreading event was $C_q = 30$ quanta/m^3. Furthermore, it suggests that the incubation time is significantly less than 12 days, as is consistent with current estimates for the average time between exposure and the onset of symptoms being 2-5 days [27].

Our fitting of I_0 and C_q for the Diamond Princess is based on the hypothesis of a "well-mixed ship". While such an approach is not traditional, and would be contested by those who do

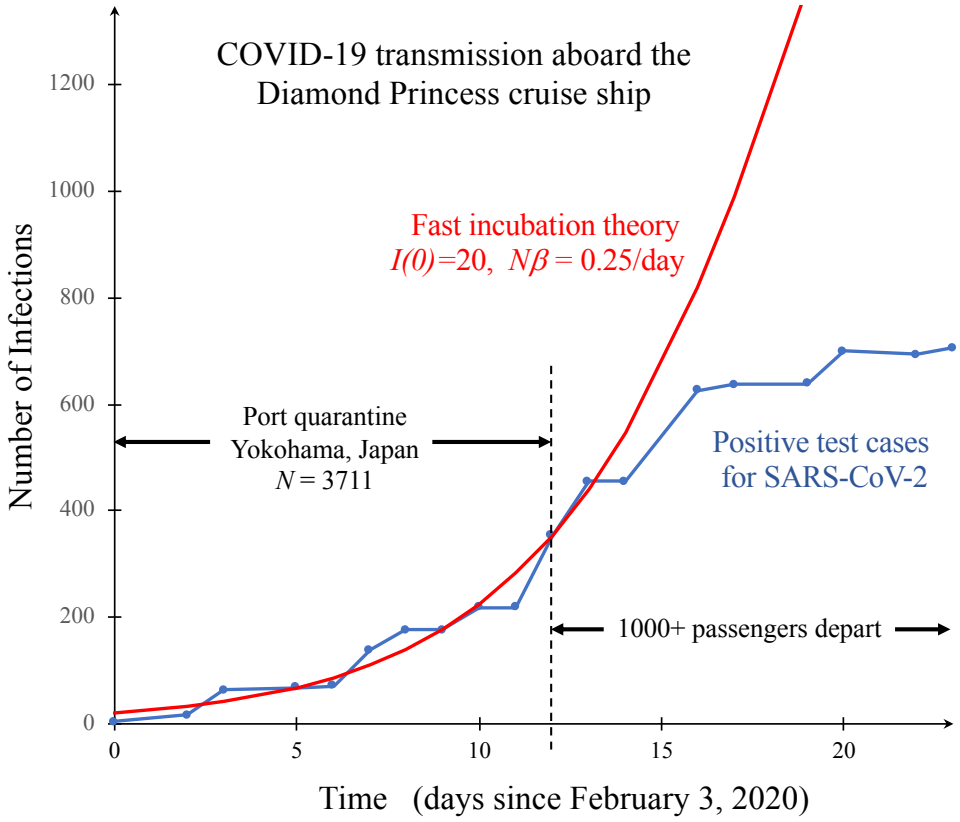

Figure S1: Validation and calibration of the fast-incubation model for the super-spreading event on board the Diamond Princess cruise ship, during its twelve day quarantine at Yokohama, Japan in February 2020 [3]. Fitting the number of SARS-CoV-2 positive cases versus time (blue data points) during the quarantine period, to the fast-incubation solution of the SEI model, Eq. (S3), (red curve) yields estimates for the initial number infected ($I_0 = 20$) and the transmission rate ($N\beta = 0.25$/day), from which we infer the concentration of infection quanta from breathing ($C_q = 30$ quanta/m^3). The relevant physical parameters are listed in Table S1.

	N	τ (h)	I_0	$I(\tau)$	λ_a (1/h)	A (m^2)	H (m)	Q_b (m^3/h)	C_q (q/m^3)
Church Choir	61	2.5	1	53	0.65	180	4.5	1.0	870
Cruise Ship	3711	288	20	354	8	139,000	2.1	0.5	30
Wuhan Apartment	3.03	132	1	1.63	0.34	90	2.4	0.5	29

Table S1: Data from three COVID-19 spreading events used to infer the concentration of exhaled infection quanta, C_q, on the basis of the assumption of indoor airborne transmission. **1.** The Skagit Valley Choir event [15]. We use existing estimates of relevant physical parameters [26] and the Wells-Riley model [17–20,26], Eq. (S2), appropriate for slow incubation, . **2.** Diamond Princess (Cruise Ship) during its 12-day port quarantine in Yokohama, Japan [3,4]. We infer $I_0 = 20$ and $N\beta = 0.25/\text{day}$ by fitting the confirmed case history to our fast-incubation solution, Eq. (S3), as shown in Fig. S1. We estimate relevant volume and area from floor plans of the Diamond Princess [6,28], where passengers and crew mainly occupy 14 floors of living space of beam width 38 m, an average length equal to 90% of the ship's length 290 m, and mean ceiling height 2.1 m. We also assume a standard cruise-ship ventilation rate (8 ACH) for partially recirculated air conditioning [29]. **3.** Initial outbreak in Wuhan, China (Wuhan Apartment). We assume that the population-level spreading is dominated by indoor aerosol transmission with slow incubation (Eq. S2) in single-family apartments [30] with a mean family size of 3.03 [31], mean apartment area of 315 SF/person [32] and ventilation rate of 0.34 ACH [33]. We estimate a mean exposure time of $\tau = 5.5$ days until symptoms (and patient isolation), and use the average $\mathcal{R}_0 = 3.3$ estimated for the population during the initial outbreak [34] in place of $\mathcal{R}_{in}(\tau)$.

not believe that airborne transmission was prevalent on the Diamond Princess [35], it is consistent with a growing body of evidence [36]. Analysis of the ship's floor plans and ventilation system has indicated recirculation of heated interior air throughout the entirety of the ship during cold weather (-5° C), without adequate filtration for virus-containing aerosol droplets [5,6]. Moreover, a detailed statistical analysis of the SARS-CoV-2 transmission history between passenger cabins revealed no significant correlation between new cases and the sharing of rooms with previously confirmed cases. Airborne transmission was further suggested by several examples of new cases emerging in single-occupancy cabins despite no known contact with other cases [5]. Like many other indoor COVID-19 spreading events [37] in which position in an enclosed space was uncorrelated with likelihood of transmission [38], the cruise line outbreaks present evidence that strongly supports the notion of airborne transmission of SARS-CoV-2 through well-mixed spaces [39,40].

Other spreading events. Table S1 shows the data used to infer the concentration of infection quanta C_q exhaled by an infected individual for two well-known indoor super-spreading events of COVID-19: the Skagit Valley Choir event [15,26], and the Diamond Princess, which we describe in terms of the slow- and fast-incubation limits, respectively. Unlike many other relatively incomplete reports of indoor spreading events, the physical parameters in these two cases can be estimated with reasonable accuracy from published data. In both situations, we assume an effective particle radius $\overline{r} = 2.0\mu$m at the upper limit of the infectious range of suspended droplets [41], corresponding to an effective settling speed of $v_s(\overline{r}) = 1.78$ m/h. Note that the effective radius would be somewhat larger, $\overline{r} = 3.0\mu$m, if we were to neglect the size dependence of infectivity and set n_q =constant, and use our prediction of the steady-state airborne droplet distribution $C_s(r)/c_v$ for singing in

the choir room (Fig. 1). We also assume no use of face masks, $p_m = 1$ and an airborne virus deactivation rate, $\lambda_v = 0.3$/h [26] that lies between estimates of zero [42] and 0.63/h [38]

Table S1 also shows how the theory can be used to interpret the population-level reproductive number in terms of indoor airborne transmission, assuming that the primary disease transmission arises in family apartments, as shown in a recent analysis of COVID-19 spreading in China [30]. We consider the initial outbreak in Wuhan, Hubei Province and assume physical parameters appropriate for typical apartments and families. We then use the average population reproductive number [34] to assert $\mathcal{R}_{in}(\tau) = \langle \mathcal{R}_0 \rangle = 3.3$, where $\tau = 5.5$ days is the mean time for an newly infected family member to show symptoms and be isolated or removed.

As shown in the main text (Fig.2), the inferred values of $C_q = 29$ quanta/m^3 for family apartments in the Wuhan outbreak and $C_q = 30$ quanta/m^3 for the Diamond Princess cruise ship are consistent with the light respiratory activities expected to be most prevalent in those settings, such as sleeping and quiet speech. Both inferred C_q values are greatly exceeded by the inference of $C_q = 870$ (made here, using $\bar{r} = 2.0\mu$m and $\lambda_a = 0.65$/h; see Table S1) or 970 quanta/m^3 (made by Miller et al [26], averaging over simulations with variable $\lambda_a = 0.3 - 1.0$/h and $\lambda_s = 0.3 - 1.5$/h) for singing, but in a manner consistent with the increased pathogen output associated with more vigorous speaking or singing [43,44]. These inferences (and others [45]) build confidence in our estimates of exhaled quanta concentrations, C_q, for various respiratory activities, as shown in Figure 2 of the main text.

Activity	Experiment [46]	Q_b (m^3/h)	ϕ_1 (10^{-16})	C_q (q/m^3)	λ_q (q/h)
breathing at rest	nose in, nose out (b-nn)	0.5	0.35	8.8	4.2
breathing heavily	nose in, mouth out (b-nm)	0.5	1.3	33	16
whispering	whispered counting (c-w-p)	0.75	1.5	37	28
speaking	voiced counting (c-v-p)	0.75	2.9	72	54
singing softly	whispered "aahs" (aah-w-p)	1.0	4.1	103	103
singing	voiced "aahs" (aah-v-p)	1.0	39	970 [26]	970

Table S2: Activity dependence of airborne transmission of COVID-19. Expiratory droplet size distributions for different activities are taken from the experiments reported by Morawska et al. [46], and reasonable estimates are made for the exhaled air volume per time Q_b from breathing (0.5 m^3/h), speaking (0.75 m^3/h) and singing (1.0 m^3/h). Our model is then used to predict the steady-state aerosol volume fraction, $\phi_1 = \int_0^{r_c} \phi_s(r)\, dr$, that results from exhalation of a single infectious individual in a setting corresponding to the Skagit Valley Choir room (Table S1), by integrating the distributions shown in Fig. 1 up to the critical radius $r_c = 2.5\mu$m. The concentration of COVID-19 infection quanta in the breath of an infected individual is assumed to be $C_q = 970$ q/m^3 for the singing case, as estimated for the Skagit Valley Chorale incident by Miller et al. [26], and values of C_q for other activities are calculated by rescaling with the appropriate ratio of aerosol volume fractions, ϕ_1. The quanta emission rate for each activity is then given by $\lambda_q = Q_b C_q$.

S3 The dependence of airborne disease transmission on respiratory activity

It is well established that aerosol droplet production varies strongly with the form of expiratory activity [46,47]. For example, vocalization greatly increases aerosol emission relative to quiet breathing, roughly in proportion to the amplitude of the sound produced [44,48]. In Table S2, the aerosol volume fraction produced by different activities, obtained by integrating the distributions in Fig. 1 up to $r_c = 2.5\mu$m, are used to rescale the inferred quanta concentration for singing [26] in the Skagit Valley Choir room into those appropriate for other activities. The resulting values are consistent with the values of C_q inferred for the Diamond Princess quarantine and the initial Wuhan City outbreak (see Table S1 and Fig. 2).

S4 Application of the Safety Guideline

In order to illustrate how to implement our safety guideline, we provide an Excel spreadsheet, COVID-19_Indoor_Safety_Guideline.xlsx, as Supplementary Data. This spreadsheet enables the calculation of the suggested maximum cumulative exposure times for specific indoor spaces. In this section, we offer guidance on how to use the spreadsheet for both safety assessment and contact tracing, specifically, how to select suitable parameters and properly interpret the results. The input parameters, colored in pink in the spreadsheet and in *italics* below, are divided into the following four categories.

Physical Parameters. The geometry of the indoor space is specified by its *floor area* A and *mean ceiling height* H, from which the volume $V = AH$ is calculated using appropriate unit conversions.

The ventilation flow rate $Q = V\lambda_a$ is calculated from the *air exchange rate*, or air changes per hour (ACH), λ_a. This critical input parameter is governed by national or local standards for different types of indoor spaces, such as the ASHRAE standards in the United States [49]. Typical values are tabulated on Wikipedia [50] and other on-line references. As noted in the main text, natural ventilation may be approximated as $\lambda_a = 0.34$/h, which has been measured in bedrooms with closed windows [33] and is considered to be the minimum standard [49], although this value will vary with both location and quality of construction. Mechanical ventilation for residences, classrooms, businesses, and public spaces usually falls in the range $\lambda_a = 4-8$/h. Crowded spaces, such as bars, nightclubs and restaurants, often require more vigorous ventilation, $\lambda_a = 15 - 20$/h. Minimum ventilation standards for American hospitals have increased from 12 to 18 ACH [51]. Most chemical and biological laboratories have λ_a in the range of $6 - 12$/h, but those handling toxic or infectious materials may have λ_a as high as $20 - 30$/h.

Physiological Parameters. The first physiological parameter is the volumetric *breathing flow rate*, Q_b, which is approximately 0.5 m^3/h for resting and light activity. Average values for healthy males and females have been reported as 0.49, 0.54, 1.38, 2.35, and 3.30 m^3/h for resting, standing, light exercise, moderate exercise and heavy exercise, respectively [52], and used in simulations of airborne transmission of COVID-19 [18]. The second physiological parameter is the mean *respiratory aerosol droplet size* $\bar{r}$ for the suspended infectious droplets responsible for airborne disease transmission. The precise definition of $\bar{r}$ is given in Eqs. (4) and (11) of the main text, in terms of the distribution of droplet sizes for different types of respiration [44,46,48], the size-dependent infectivity of aerosol droplets [41], and the settling and ventilation rates. However, as illustrated in the

main text, a typical value for the most common and most infectious droplets is $\bar{r} = 2 - 3\mu$m. We note that these values are roughly consistent with the standard definition of aerosol droplets, as those having $r < 5\mu$m [18].

Disease Parameters. The most important disease parameter is the *infectiousness of exhaled air* C_q (infection quanta per volume), as discussed extensively in the main text. Using all of the limited information currently available, we estimate $C_q = 30$ q/m^3 for normal breathing and light activity and provide our best estimates of C_q for different respiratory activities in Fig. 2. Our analysis indicates that C_q can be an order of magnitude larger for singing or other vigorous respiratory activity, or an order of magnitude smaller for sleeping and light nose breathing. The second disease parameter is the *viral deactivation rate*, λ_v, at which the aerosol-bound virus loses infectiousness, which for SARS-CoV-2 has been estimated to lie in the range of zero [42] to 0.63/h [38]. We note that deactivation rates may be enhanced by ultraviolet radiation (UV-C) [53], chemical disinfectants (*e.g.* H_2O_2, O_3) [54], or high-efficiency particulate air (HEPA) filtration [55].

Precautionary Parameters. The first precautionary parameter is the *mask filtration factor*, p_m, defined as the fraction of infectious aerosol droplets that pass through the mask during exhalation or inhalation. Many studies are available to help assign this value for different types of face coverings, ranging from cloth coverings to surgical masks [56–59]. Although filtration efficiency depends on drop size, it is typically nearly constant in the aerosol range [56,57]. Typical values for disposable medical masks are in the range $p_m = 1 - 5\%$ [57,58], while for simple cloth face masks, $p_m = 10 - 20\%$ [59].

The second precautionary parameter is the *disease transmission tolerance*, ϵ. We note that

$\epsilon = 1$ corresponds to the baseline of one expected transmission during the occupancy period. The choice of ϵ should take into account the vulnerability of the population, which for COVID-19 is a strong function of age and pre-existing medical conditions [27,60,61]. Relative to the median age of 69 in the Skagit Valley Chorale spreading incident, used to calibrate our model, the relative rate of hospitalization with COVID-19 [60] can be calculated as 2.5% (ages 0-4), 0.8% (ages 5-17), 20% (ages 18-49), 61% (ages 50-64), 130% (ages 75-84), and 145% (ages > 85). For the elderly, especially those with pre-existing conditions or co-morbidity, $\epsilon \ll 1$ should be chosen. For the young and healthy (in regions where hospitals are not overwhelmed and vulnerable groups are protected), larger values of ϵ could be considered [62]. As noted in the main text, choosing a sufficiently small ϵ will also serve to mitigate against prolonged exposure to respiratory jets, whose contribution to pathogen transport may dominate in the absence of face-mask use [63].

Results. The spreadsheet first computes properties of the infectious aerosol per infected individual in the room, which are primarily of technical interest: the effective droplet settling speed $v_s(\bar{r})$, the concentration relaxation rate $\lambda_c(\bar{r})$, the dilution factor, f_d, and the infectiousness of the ambient air, $f_d C_q$, in steady state per infected person in the room.

The spreadsheet computes the safety guideline in two ways with the key results highlighted in green. First, the occupancy limit N_{max} can be calculated for a given *indoor exposure time* τ, as is set by the typical residence time of persons in the space. Second, the time limit τ_{max} can be calculated for a given *occupancy* N. These bounds are plotted and may be compared to the Six-Foot Rule and 15-Minute Rule, both of which invariably violate our guideline.

Contact Tracing. The spreadsheet can also be used as a tool for contract tracing. Using a conservative tolerance, such as $\epsilon = 0.01$, which guards against airborne transmission. the guideline defines whether or not the N occupants of a room visited by the index case for a time τ should be considered as contacts for the purpose of tracing the infection network. If the guideline is violated, then *all* occupants of the room must be considered contacts, regardless of their distance from the index case.

References

1. Lauer, S. A. *et al.* The incubation period of coronavirus disease 2019 (COVID-19) from publicly reported confirmed cases: estimation and application. *Annals of internal medicine* **172**, 577–582 (2020).

2. Ito, H., Hanaoka, S. & Kawasaki, T. The cruise industry and the COVID-19 outbreak. *Transportation Research Interdisciplinary Perspectives* 100136 (2020).

3. Moriarty, L. F. Public health responses to COVID-19 outbreaks on cruise ships worldwide, February–March 2020. *MMWR. Morbidity and Mortality Weekly Report* **69** (2020).

4. Kakimoto, K. *et al.* Initial investigation of transmission of COVID-19 among crew members during quarantine of a cruise ship, Yokohama, Japan, February 2020. *MMWR. Morbidity and Mortality Weekly Report* **69** (2020).

5. Almilaji, O. & Thomas, P. Air recirculation role in the infection with covid-19, lessons learned from diamond princess cruise ship. *medRxiv preprint* (2020).

6. Ege, I. The impact of coronavirus disease (covid-19) pandemic on cruise industry: Case of diamond princess cruise ship. *Mersin University Journal of Maritime Faculty* **2**, 32–37 (2020).

7. Dyal, J. W. COVID-19 among workers in meat and poultry processing facilities: 19 states, april 2020. *MMWR. Morbidity and Mortality Weekly Report* **69** (2020).

8. Waltenburg, M. A. Update: COVID-19 among workers in meat and poultry processing facilities: United states, april–may 2020. *MMWR. Morbidity and Mortality Weekly Report* **69** (2020).

9. Hawks, L., Woolhandler, S. & McCormick, D. Covid-19 in prisons and jails in the united states. *JAMA Internal Medicine* (2020).

10. Kinner, S. A. *et al.* Prisons and custodial settings are part of a comprehensive response to COVID-19. *The Lancet Public Health* **5**, e188–e189 (2020).

11. Noakes, C., Beggs, C., Sleigh, P. & Kerr, K. Modelling the transmission of airborne infections in enclosed spaces. *Epidemiology & Infection* **134**, 1082–1091 (2006).

12. Bootsma, M. C. & Ferguson, N. M. The effect of public health measures on the 1918 influenza pandemic in US cities. *Proceedings of the National Academy of Sciences* **104**, 7588–7593 (2007).

13. Bertozzi, A. L., Franco, E., Mohler, G., Short, M. B. & Sledge, D. The challenges of modeling and forecasting the spread of covid-19. *arXiv preprint arXiv:2004.04741* (2020).

14. Kermack, W. O. & McKendrick, A. G. A contribution to the mathematical theory of epidemics. *Proc. Roy. Soc. London. Series A* **115**, 700–721 (1927).

15. Hamner, L. High SARS-CoV-2 attack rate following exposure at a choir practice, Skagit County, Washington, March 2020. *MMWR. Morbidity and Mortality Weekly Report* **69** (2020).

16. Harko, T., Lobo, F. S. & Mak, M. Exact analytical solutions of the susceptible-infected-recovered (SIR) epidemic model and of the sir model with equal death and birth rates. *Applied Mathematics and Computation* **236**, 184–194 (2014).

17. Gammaitoni, L. & Nucci, M. C. Using a mathematical model to evaluate the efficacy of TB control measures. *Emerging Infectious Diseases* **3**, 335 (1997).

18. Buonanno, G., Stabile, L. & Morawska, L. Estimation of airborne viral emission: quanta emission rate of SARS-CoV-2 for infection risk assessment. *Environment International* **141**, 105794 (2020).

19. Wells, W. F. *et al.* Airborne contagion and air hygiene. an ecological study of droplet infections. *Airborne Contagion and Air Hygiene. An Ecological Study of Droplet Infections.* (1955).

20. Riley, E. C., Murphy, G. & Riley, R. L. Airborne spread of measles in a suburban elementary school. *American Journal of Epidemiology* **107**, 421–432 (1978).

21. Beggs, C., Noakes, C., Sleigh, P., Fletcher, L. & Siddiqi, K. The transmission of tuberculosis in confined spaces: an analytical review of alternative epidemiological models. *The international journal of tuberculosis and lung disease* **7**, 1015–1026 (2003).

22. Watanabe, T., Bartrand, T. A., Weir, M. H., Omura, T. & Haas, C. N. Development of a dose-response model for SARS coronavirus. *Risk Analysis* **30**, 1129–1138 (2010).

23. Knibbs, L. D., Morawska, L. & Bell, S. C. The risk of airborne influenza transmission in passenger cars. *Epidemiology & Infection* **140**, 474–478 (2012).

24. Liao, C.-M., Chang, C.-F. & Liang, H.-M. A probabilistic transmission dynamic model to assess indoor airborne infection risks. *Risk Analysis* **25**, 1097–1107 (2005).

25. Rudnick, S. & Milton, D. Risk of indoor airborne infection transmission estimated from carbon dioxide concentration. *Indoor air* **13**, 237–245 (2003).

26. Miller, S. L. *et al.* Transmission of SARS-CoV-2 by inhalation of respiratory aerosol in the Skagit Valley Chorale superspreading event. *medRxiv preprint* (2020).

27. Davies, N., Klepac, P., Liu, Y. *et al.* Age-dependent effects in the transmission and control of COVID-19 epidemics. *Nature Medicine* **898** (2020).

28. Https://www.cruisedeckplans.com/DP/deckplans/Diamond-Princess (accessed on July 14, 2020).

29. Zheng, L., XU, J., WU, F., XU, W. & LONG, Z. Influences of ventilation modes on the coughing droplet dispersion process in a cruise cabin. *Chinese Journal of Ship Research* **11** (2016).

30. Qian, H. *et al.* Indoor transmission of sars-cov-2. *medRxiv preprint* (2020).

31. Https://www.statista.com/statistics/278697/average-size-of-households-in-china (accessed on June 28, 2020).

32. Orlik, T. In China, a move to tiny living space. *Wall Street Journal* **July 11** (2020).

33. Hou, J. *et al.* Air change rates in urban Chinese bedrooms. *Indoor air* **29**, 828–839 (2019).

34. Liu, Y., Gayle, A. A., Wilder-Smith, A. & Rocklöv, J. The reproductive number of COVID-19 is higher compared to SARS coronavirus. *Journal of Travel Medicine* **27**, 1–4 (2020).

35. Xu, P. *et al.* Transmission routes of COVID-19 virus in the Diamond Princess cruise ship (2020). URL https://www.medrxiv.org/content/early/2020/04/14/2020.04.09.20059113.

36. Azimi, P. *et al.* Mechanistic transmission modeling of COVID-19 on the diamond princess cruise ship demonstrates the importance of aerosol transmission (2020). URL https://www.medrxiv.org/content/early/2020/07/15/2020.07.13.20153049.

37. Nishiura, H. *et al.* Closed environments facilitate secondary transmission of coronavirus disease 2019 (COVID-19). *medRxiv preprint* (2020).

38. Van Doremalen, N. *et al.* Aerosol and surface stability of SARS-CoV-2 as compared with SARS-CoV-1. *New England Journal of Medicine* **382**, 1564–1567 (2020).

39. Morawska, L. & Milton, D. K. It is time to address airborne transmission of COVID-19. *Clinical Infectious Diseases* ciaa939 (2020).

40. Morawska, L. & Cao, J. Airborne transmission of SARS-CoV-2: The world should face the reality. *Environment International* **139**, 105730 (2020).

41. Santarpia, J. L. *et al.* The infectious nature of patient-generated SARS-CoV-2 aerosol. *medRxiv preprint* (2020).

42. Fears, A. C. *et al.* Comparative dynamic aerosol efficiencies of three emergent coronaviruses and the unusual persistence of SARS-CoV-2 in aerosol suspensions. *medRxiv preprint* (2020).

43. Morawksa, L. Droplet fate in indoor environments, or can we prevent the spread of infection? *Indoor Air* **16**, 335–347 (2006).

44. Asadi, S. *et al.* Aerosol emission and superemission during human speech increase with voice loudness. *Scientific Reports* **9**, 1–10 (2019).

45. Bazant, M. Z. Theory of indoor disease transmission with applications to covid-19 In preparation.

46. Morawska, L. *et al.* Size distribution and sites of origin of droplets expelled from the human respiratory tract during expiratory activities. *Journal of Aerosol Science* **40**, 256–269 (2009).

47. Bake, B., Larsson, P., Ljungkvist, G., Ljungström, E. & Olin, A. Exhaled particles and small airways. *Respiratory research* **20**, 8 (2019).

48. Asadi, S. *et al.* Effect of voicing and articulation manner on aerosol particle emission during human speech. *PloS one* **15**, e0227699 (2020).

49. *Ventilation and Acceptable Indoor Air Quality in Residential Buildings* (American Society of Heating, Refrigerating and Air-Conditioning Engineers, 2016). ASHRAE Standard 62.2.

50. *Air Exchanges Per Hour* (2020 (accessed June 10, 2020)). Https://en.wikipedia.org/wiki/Air_changes_per_hour.

51. Ninomura, P. & Bartley, J. New ventilation guidelines for health-care facilities. *ASHRAE journal* **43**, 29 (2001).

52. Adams, W. C. *Measurement of breathing rate and volume in routinely performed daily activities: Final report, contract no. A033-205* (California Air Resources Board, Sacramento, CA, 1993).

53. García de Abajo, F. J. *et al.* Back to normal: An old physics route to reduce sars-cov-2 transmission in indoor spaces. *ACS nano* **14**, 7704–7713 (2020).

54. Schwartz, A. *et al.* Decontamination and reuse of n95 respirators with hydrogen peroxide vapor to address worldwide personal protective equipment shortages during the sars-cov-2 (covid-19) pandemic. *Applied Biosafety* **25**, 67–70 (2020).

55. Mousavi, E. S., Pollitt, K. J. G., Sherman, J. & Martinello, R. A. Performance analysis of portable hepa filters and temporary plastic anterooms on the spread of surrogate coronavirus. *Building and Environment* 107186 (2020).

56. Chen, C.-C. & Willeke, K. Aerosol penetration through surgical masks. *American journal of infection control* **20**, 177–184 (1992).

57. Oberg, T. & Brosseau, L. M. Surgical mask filter and fit performance. *American journal of infection control* **36**, 276–282 (2008).

58. Li, Y. *et al.* Transmission of communicable respiratory infections and facemasks. *Journal of multidisciplinary healthcare* **1**, 17 (2008).

59. Konda, A. *et al.* Aerosol filtration efficiency of common fabrics used in respiratory cloth masks. *ACS Nano* **14**, 6339–6347 (2020).

60. Garg, S. Hospitalization rates and characteristics of patients hospitalized with laboratory-confirmed coronavirus disease 2019: COVID-NET, 14 States, March 1–30, 2020. *MMWR. Morbidity and Mortality Weekly Report* **69** (2020).

61. Ioannidis, J. P., Axfors, C. & Contopoulos-Ioannidis, D. G. Population-level COVID-19 mortality risk for non-elderly individuals overall and for non-elderly individuals without underlying diseases in pandemic epicenters. *medRxiv preprint* (2020).

62. COVID-19 Planning Considerations: Guidance for School Re-entry, American Academy of Pediatrics, June 25, 2020. https://services.aap.org/en/pages/2019-novel-coronavirus-covid-19-infections/clinical-guidance/covid-19-planning-considerations-return-to-in-person-education-in-schools/.

63. Chen, W., Zhang, N., Wei, J., Yen, H.-L. & Li, Y. Short-range airborne route dominates exposure of respiratory infection during close contact. *Building and Environment* 106859 (2020).